Research Square

Preprints are preliminary reports that have not undergone peer review.
They should not be considered conclusive, used to inform clinical practice,
or referenced by the media as validated information.

Dynamic elasticity modulus evolution and mechanical performance of cement mortars incorporating eggshell and rice husk ashes: A phenomenological Avrami-type approach

G. C. Ribeiro[1]

girribeiro@yahoo.com.br

Universidade de São Paulo

G. R. Z. Garcia[2]

COTEL

T. L. F. Mafra[2]

COTEL

T. M. Ribeiro[3]

Universidade Estadual Paulista (Unesp)

S. Ribeiro[1]

Universidade de São Paulo

Article

Keywords: eggshell ash, rice husk ash, cement mortar, dynamic elastic modulus, stiffness development, Avrami-type modeling

Posted Date: November 16th, 2026

DOI: https://doi.org/10.21203/rs.3.rs-11528470/v1

License: This work is licensed under a Creative Commons Attribution 4.0 International License.
Read Full License

Additional Declarations: No competing interests reported.

Dynamic elasticity modulus evolution and mechanical performance of cement mortars incorporating eggshell and rice husk ashes: A phenomenological Avrami-type approach

G. C. Ribeiro[1],*, G. R. Z. Garcia[2], T. L. F. Mafra[2], T. M. Ribeiro[3], S. Ribeiro[1]

[1] School of Engineering of Lorena, University of São Paulo (EEL/USP), Lorena, São Paulo, Brazil.

[2] Lorena Technical School – Prof. Nelson Pesciota (COTEL), Lorena, São Paulo, Brazil.

[3] School of Engineering, São Paulo State University (UNESP), Guaratinguetá, São Paulo, Brazil.

*Corresponding author: G. C. Ribeiro

E-mail: girribeiro@yahoo.com.br

Abstract

The incorporation of agro-industrial ashes into cement mortars offers opportunities for waste valorization, but their effects on time-dependent stiffness development and final mechanical performance require integrated assessment. This study investigated eggshell ash (ESA) and rice husk ash (RHA) added individually at 5% and 10% of cement mass, without cement replacement, using a constant water-to-cement ratio of 0.56. Dynamic elastic modulus was monitored daily for 28 days through nondestructive resonance testing. Normalized stiffness trajectories were fitted using a generalized phenomenological Avrami-type model, while physical properties and mechanical strengths were evaluated at 28 days. Both 5% formulations exhibited faster relative stiffness development than the reference, with characteristic t_{90} values of 5.78 days for ESA and 5.51 days for RHA, compared with 6.19 days for the reference. However, their final mechanical responses differed. The 5% ESA formulation reduced water absorption by 14.4% and apparent porosity by 15.6%, while maintaining dynamic elastic modulus (21.65 GPa) and compressive strength (23.70 MPa) close to reference values (22.31 GPa and 23.76 MPa, respectively). In contrast, 5% RHA maintained comparable stiffness but exhibited lower compressive strength. At 10% incorporation, both ashes produced greater reductions in mechanical performance. These findings demonstrate that faster normalized stiffness development does not necessarily imply superior final strength. Integrating nondestructive monitoring, phenomenological modeling, and conventional testing provides a complementary framework for evaluating ash-containing mortars and supports low-dosage waste valorization without assuming direct cement replacement or verified environmental benefits.

Keywords: eggshell ash; rice husk ash; cement mortar; dynamic elastic modulus; stiffness development; Avrami-type modeling.

1. Introduction

The environmental impacts associated with the construction industry have encouraged the development of cement-based materials that promote more efficient resource utilization and the valorization of industrial and agricultural residues. Portland cement is the primary binder used in mortars and concrete. However, its production is associated with substantial carbon emissions, mainly due to limestone decarbonation during clinker manufacture and the energy required for high-temperature processing [1–4]. In this context, the incorporation of agro-industrial residues into cementitious matrices has attracted increasing attention as a strategy for valorizing secondary raw materials and modifying the physical and mechanical properties of cement-based composites [5–7].

Among the available agro-industrial residues, eggshells and rice husks are particularly relevant because of their distinct chemical compositions and potential applications in cementitious materials. Eggshells consist predominantly of calcium carbonate ($CaCO_3$), whereas rice husks contain organic matter and a mineral fraction rich in silica [8–11]. Rice production is particularly significant in Brazil, highlighting the relevance of investigating alternative applications for residues generated during agricultural processing [12]. Following appropriate thermal treatment, these materials can be converted into ashes with different chemical and mineralogical characteristics, which may influence the behavior of cement mortars.

Calcination of eggshells at sufficiently high temperatures promotes the decomposition of $CaCO_3$ into calcium oxide (CaO) [10,11]. Previous investigations have shown that eggshell-derived materials can affect cement hydration and the physical and mechanical properties of cementitious systems, depending on processing conditions, particle characteristics, and incorporation levels [13–18]. In contrast, controlled calcination of rice husks can produce ash containing a high proportion of amorphous or poorly crystalline silica, a characteristic associated with potential pozzolanic reactivity [8,19]. Studies have reported that rice husk ash (RHA) can modify the microstructure and mechanical properties of cement-based materials, although the magnitude of these effects depends on ash characteristics and matrix composition [19,20].

These compositional differences justify investigating the individual effects of eggshell ash (ESA) and RHA on cement mortars at different incorporation levels. However, evaluating the performance of ash-containing mortars solely through properties measured at selected curing ages provides limited information about their mechanical development. The temporal evolution of stiffness offers an additional perspective on the progressive formation of a load-bearing solid structure during curing.

Stiffness development in cementitious materials is associated with cement hydration and the progressive formation of an interconnected solid network. Dissolution and precipitation reactions produce hydrated phases, particularly calcium silicate hydrate (C–S–H), which contribute to the development of cohesion and mechanical properties [1,2]. Nevertheless, the elastic response of mortars and concrete also depends on porosity, solid-phase connectivity, matrix composition, and aggregate characteristics. Consequently, changes in elastic modulus cannot be directly equated with changes in the degree of cement hydration.

Nondestructive measurements of dynamic elastic modulus provide an opportunity to monitor mechanical development throughout curing while preserving specimens for repeated testing. Zhao et al. [21] demonstrated the application of this approach to monitoring the early-age dynamic modulus of cement pastes. Similarly, Valentini et al. [22] investigated relationships between hydration-related phase evolution and the development of elastic moduli in cementitious materials through experimental characterization and microstructural modeling. These studies support the use of dynamic elastic modulus as a mechanical indicator of structural development, although its evolution does not constitute a direct measurement of chemical hydration kinetics.

Mathematical descriptions of time-dependent processes in cementitious systems have included models derived from the Avrami–Erofeev formalism. Bezjak [23] applied this approach to cement hydration kinetics while considering different mechanistic contributions. Ma et al. [24] subsequently proposed a model combining a modified Avrami equation with a cement hydration formulation to represent different stages of system evolution. Thomas [25] and Bishnoi and Scrivener [26] also investigated nucleation-and-growth-based descriptions of cement hydration, highlighting both the relevance of these processes and the limitations of representing complex hydration behavior through a single kinetic mechanism.

Although such approaches provide a mathematical framework for describing time-dependent transformations, their application to mechanical properties requires a different interpretation from that adopted for hydration degree. When used to describe normalized dynamic elastic modulus, an Avrami-type function should be regarded as a phenomenological model of stiffness development rather than a direct representation of hydration reactions. Under this interpretation, fitted parameters characterize the relative rate and shape of the mechanical evolution curve without necessarily identifying specific nucleation, growth, or diffusion mechanisms.

Normalizing dynamic elastic modulus also enables comparisons among formulations that develop different absolute stiffness levels. This distinction is particularly important for mortars

containing agro-industrial ashes, as changes in material composition may affect both the relative rate of mechanical development and the final magnitude of stiffness. Accordingly, a formulation exhibiting faster normalized stiffness development does not necessarily achieve a higher elastic modulus or superior mechanical performance at later ages.

Although the effects of eggshell- and rice-husk-derived materials on cementitious properties have been investigated in previous studies [2,3,5,13–20], further examination of how the individual incorporation of these ashes influences the temporal evolution of mechanical response remains relevant. Combining daily nondestructive measurements of dynamic elastic modulus with normalization and phenomenological Avrami-type modeling provides a complementary approach to conventional mechanical testing at selected curing ages. This framework enables quantitative comparison of stiffness development trajectories alongside the final physical and mechanical properties of the mortars.

Therefore, this study investigated the effects of incorporating 5% and 10% ESA and RHA, expressed relative to cement mass and added without cement replacement, on the physical and mechanical properties and temporal stiffness development of cement mortars. Dynamic elastic modulus was monitored daily over 28 days, and its evolution was analyzed through normalization, phenomenological Avrami-type modeling, and calculation of the apparent stiffness development rate. Physical properties, flexural strength, and compressive strength were also determined at 28 days. The combined analysis was intended to distinguish relative stiffness development from final mechanical performance and to assess the influence of ash type and incorporation level on these complementary aspects of mortar behavior.

2. Materials and methods

2.1. Raw materials

The materials comprised CP III Portland cement, washed medium sand, chicken eggshells, rice husks, and potable water. Eggshells were collected from a restaurant, and rice husks were obtained from the Rice Producers' Cooperative of Vale do Paraíba in Guaratinguetá, São Paulo, Brazil.

2.2. Ash preparation and characterization

Eggshells and rice husks were washed, dried at 110 °C for 12 h, and ground using a blender. Thermogravimetric analyses were conducted using a NETZSCH STA 449 F3 Jupiter instrument at

10 °C/min under a gas flow of 100 cm³/min. Eggshells were analyzed from 25 to 900 °C under nitrogen, whereas rice husks were analyzed from 35 to 1000 °C under synthetic air. Eggshells were calcined at 950 °C for 2 h and rice husks at 700 °C for 3 h. The resulting ashes were passed through a 300 µm sieve; only the passing fraction was used, establishing an upper particle-size limit for the materials added to the mortars. Sieved ashes were stored in clean, tightly sealed containers until use to limit moisture uptake and contamination.

Crystalline phases were investigated by X-ray diffraction (PANalytical Empyrean; Cu Kα radiation; 40 kV, 25 mA; 2θ = 10–90°; scanning rate 1.2°/min). Chemical composition was determined by X-ray fluorescence spectroscopy (PANalytical Axios Max).

2.3. Mortar formulations and preparation

All mortars were prepared at a cement-to-sand mass ratio of 1:3 and a constant water-to-cement ratio of 0.56. Five formulations were investigated: reference without ash (0%); 5% and 10% additional ESA (A5%ESA and A10%ESA); and 5% and 10% additional RHA (A5%RHA and A10%RHA). Ash percentages refer to cement mass.

Ashes were incorporated as additional solids rather than as cement replacements; cement and water masses were therefore kept constant. Consequently, the water-to-cement ratio remained 0.56, whereas the water-to-(cement + ash) mass ratio decreased from 0.56 for the reference to approximately 0.533 and 0.509 for the 5% and 10% ash formulations, respectively.

The mortars were mixed using a laboratory mortar mixer with a nominal capacity of 5 L.

2.4. Physical and mechanical testing

Prismatic specimens measuring 150 × 25 × 25 mm were cast for dynamic elastic modulus and flexural tests, and cylindrical specimens measuring 50 × 100 mm were cast for compressive strength testing. Specimens were demolded 24 h after casting and kept in a water-saturated curing atmosphere at ambient temperature until 28 days.

For each formulation, the same five prismatic specimens were monitored daily to determine dynamic elastic modulus. At each age, specimens were temporarily removed from curing for measurement and returned immediately afterward. Measurements were performed using a ScanElastic-02 bar-resonance system (ATCP; ME-C1198-91), operating over a frequency range of 1–22 kHz and based on the principles of the sonic resonance procedure described in ASTM C1198-91 [27]. The resulting measurements were used to construct E-versus-curing-time trajectories.

After 28 days, prismatic specimens were subjected to three-point bending using an EMIC DL universal testing machine with a 5 kN load cell and a crosshead speed of 0.5 mm/s, with EN 1015-11:2019 cited as the methodological reference [28]. Compression tests were performed using an EMIC DL10000 machine with a 100 kN load cell at 0.5 mm/s, with ISO 1920-4:2020 cited as the methodological reference [29]. Water absorption, apparent porosity, and apparent density were measured following the procedure reported with reference to ASTM C642-21 [30], using five specimens per formulation for these physical measurements.

2.5. Normalization and phenomenological fitting

To compare temporal stiffness evolution among formulations with different absolute dynamic modulus values, the daily mean E(t) values from five specimens per formulation were normalized using the corresponding first- and 28th-day mean values, according to Eq. (1):

$$\alpha_{E,28}(t) = \frac{E_{(t)} - E_1}{E_{28} - E_1} \quad (1)$$

Here, $E_{(t)}$ is the mean dynamic elastic modulus at curing age t, and E_1 and E_{28} are the mean values measured on days 1 and 28. Thus, $\alpha_{E,28}=0$ on day 1 and $\alpha_{E,28}=1$ on day 28. This index describes relative stiffness evolution and does not represent the degree of hydration or chemical reaction extent. Because the first measurement was performed after 24 h, shifted time was defined as $\tau = t - 1$, so that $\tau = 0$ corresponds to the first measurement. The normalized trajectories were fitted using the generalized Avrami-type function in Eq. (2):

$$\alpha_{(E,28)}(\tau) = A\left[1 - e^{-(k\tau)^n}\right] \quad (2)$$

A is the fitted asymptote, k is an apparent rate parameter (day^{-1}), and n describes curve shape. All three parameters were estimated freely by nonlinear regression applied to the mean normalized trajectories. Fit quality was assessed using adjusted R^2. Parameter uncertainties are nonlinear-regression standard errors and do not represent between-specimen standard deviations. Since A was not constrained to unity, the fitted asymptote can differ from the experimental normalization endpoint $\alpha_{E,28}=1$.

Characteristic times t_f were calculated as the curing ages at which the fitted function reaches a fraction f of its own asymptote A:

$$t_f = 1 + \frac{[-\ln(1-f)]^{\frac{1}{n}}}{k} \quad (3)$$

Values for f = 0.50 and 0.90 define t_{50} and t_{90}, respectively. They refer to fractions of each fitted asymptote, not to 50% or 90% of the absolute dynamic elastic modulus measured at 28 days.

The apparent rate of normalized stiffness development was calculated directly from consecutive experimental mean values, independently of the fitted function:

$$\upsilon(\alpha, E, i) = \frac{\alpha_{(E,28)}(t_{i+1}) - \alpha_{(E,28)}(t_i)}{t_{i+1} - t_i} \quad (4)$$

The quantity $\upsilon(\alpha,E,i)$ (day^{-1}) represents the finite-difference change in normalized stiffness over a measurement interval and was assigned to its midpoint. Positive values indicate increasing normalized stiffness; small negative values can occur because of experimental fluctuations in repeated measurements.

Avrami-type parameters k, n, t_{50} and t_{90} were used exclusively as phenomenological descriptors of temporal mechanical development and were not interpreted as fundamental chemical hydration-rate constants or evidence of specific reaction mechanisms.

3. Results and discussion

3.1. Characterization of eggshells ash

Figure 1 presents the TG/DTG curves of dried eggshells. The total mass loss was approximately 46.75%, occurring in three main intervals. A loss of approximately 0.84% between 100 and 200 °C was associated primarily with residual moisture. Between 200 and 650 °C, a further loss of approximately 5.16% may be attributed mainly to decomposition of organic constituents and minor transformations. The predominant loss of approximately 40.75%, between 650 and 820 °C, was associated with calcium carbonate decomposition ($CaCO_3 \rightarrow CaO + CO_2$). Above approximately 820 °C, the TG curve approached a stable mass level, consistent with the completion of the main carbonate decomposition event under the experimental conditions [1,13].

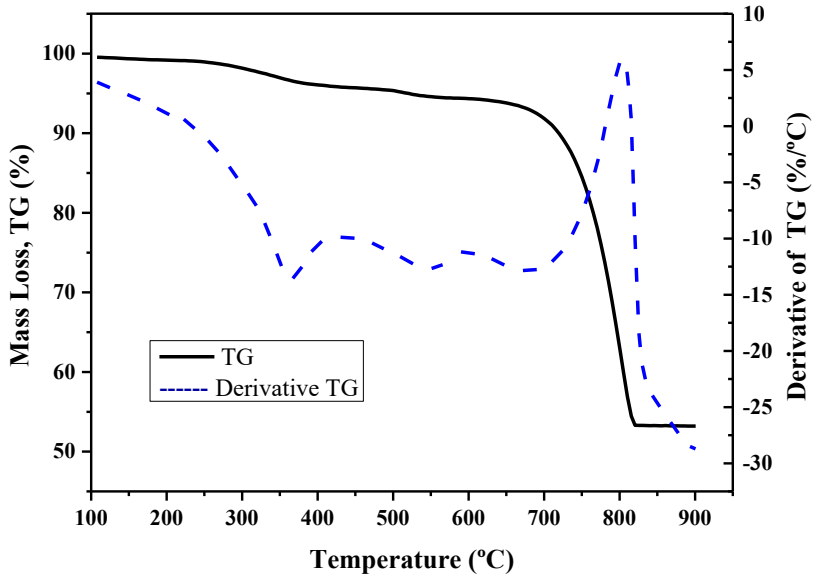


Figure 1. TG and DTG curves of dried eggshells.

The DTG curve exhibited its maximum mass-loss rate at approximately 800 °C. On this basis, eggshells were calcined at 950 °C for 2 h to produce ESA.

Figure 2 compares the XRD patterns of dried eggshells and ESA. Dried eggshells were dominated by reflections attributable to calcite ($CaCO_3$; reference ICOD 96-900-9668), whereas the ash obtained at 950 °C exhibited reflections predominantly assigned to crystalline CaO (reference ICOD 96-900-6714). This phase change is consistent with the major TG mass-loss event. The XRD results confirm the mineralogical transformation induced by calcination but do not, by themselves, establish the subsequent reactivity of ESA in the cementitious matrix.

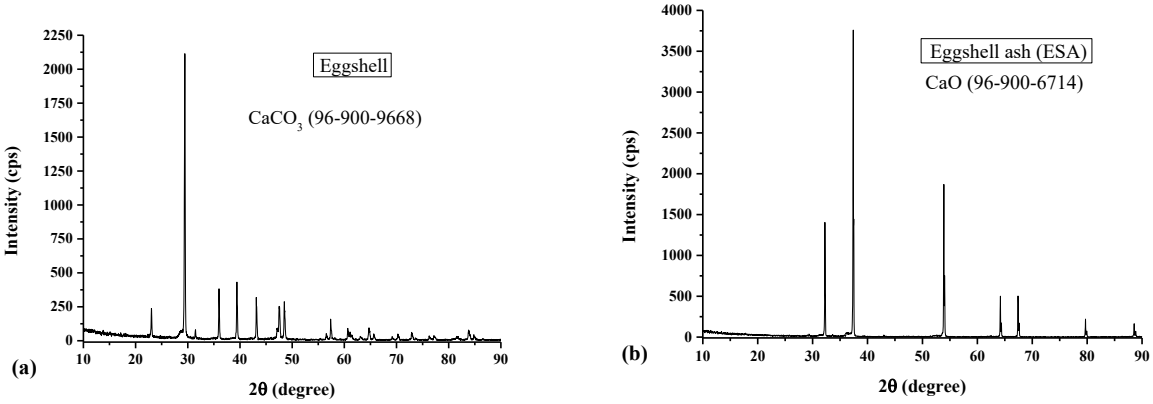


Figure 2. XRD patterns of (a) dried eggshells and (b) eggshell ash calcined at 950 °C for 2 h.

3.2. Characterization of rice husks and rice husk ash

Figure 3 shows the TG/DTG curves of rice husks under synthetic air. The initial mass loss, approximately 6.5%, was associated with moisture and volatile constituents. Subsequent decomposition and oxidation of organic matter produced a pronounced mass loss, with an overall loss of approximately 87% reported for the experiment. The DTG profile displayed a main peak near 340 °C and a broader, less intense event near 450 °C, consistent with multistage degradation under oxidizing conditions. A thermal treatment of 700 °C for 3 h was adopted to prepare RHA.

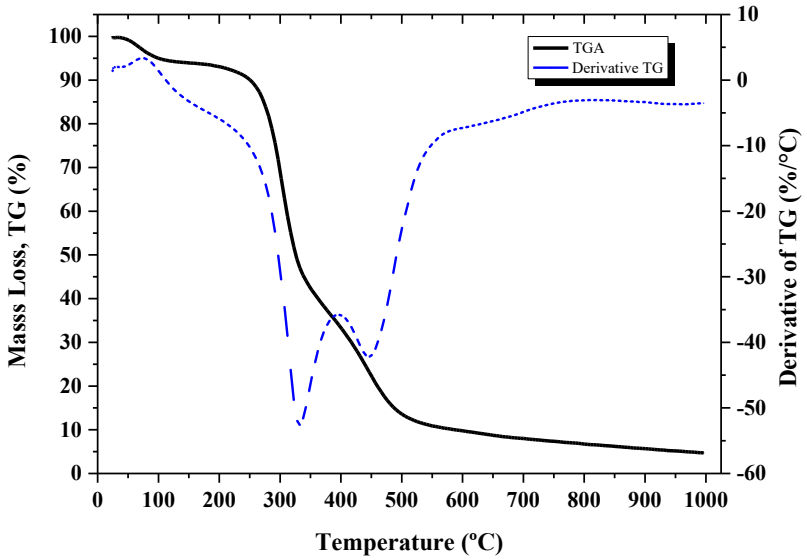


Figure 3. TG and DTG curves of rice husks under synthetic air.

XRF analysis of RHA, expressed as normalized oxide mass percentages, indicated 95.83% SiO_2. Minor constituents were K_2O (0.93%), MgO (0.80%), P_2O_5 (0.77%), CaO (0.54%), SO_3 (0.40%), Al_2O_3 (0.35%), Na_2O (0.20%), Fe_2O_3 (0.09%), MnO (0.08%), and NiO (0.01%). The high silica content establishes the silica-rich character of the ash but does not alone demonstrate pozzolanic activity.

The XRD pattern (Figure 4) displayed a broad diffuse halo approximately between 15° and 30° (2θ), consistent with a substantial amorphous or poorly crystalline fraction. Together with the XRF results, this observation is compatible with poorly crystalline silica in RHA. Such silica may be

relevant to pozzolanic potential [8,19], although neither the amorphous fraction nor pozzolanic reactivity was directly quantified in the present study.

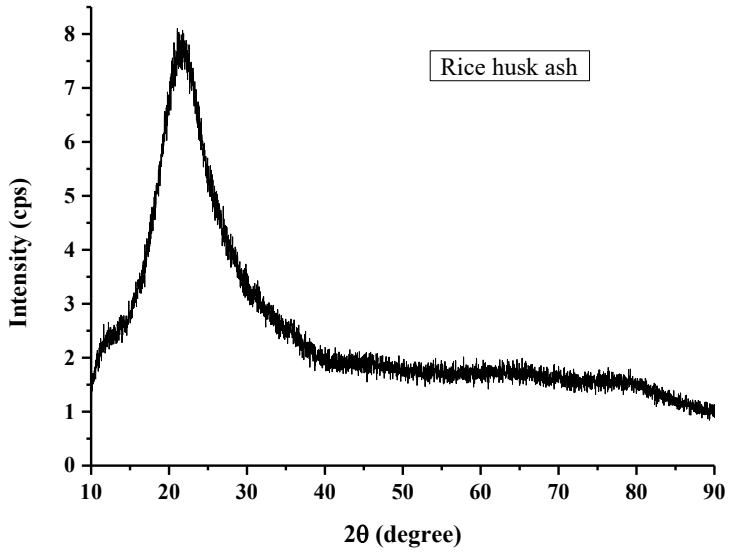


Figure 4. XRD pattern of rice husk ash calcined at 700 °C for 3 h.

3.3. Temporal development of dynamic elastic modulus

Figure 5 presents the development of dynamic elastic modulus over 28 days. All formulations showed a pronounced initial increase followed by a progressive reduction in the rate of modulus development. The first available interval, between days 1 and 2, showed the largest measured increment. Subsequent increases became smaller as curing progressed, and the trajectories tended toward comparatively stable values at later ages. This response is compatible with progressive development of a load-bearing solid structure, although dynamic modulus is influenced by several material characteristics and cannot be used as a direct measure of hydration kinetics [21,22].

The reference, A5%ESA, and A5%RHA formulations generally exhibited the highest absolute stiffness trajectories. By contrast, 10% ash incorporation resulted in lower modulus values over much of the curing period, particularly for A10%RHA.

Although the overall trajectory shapes were similar, the magnitudes and relative rates of stiffness development differed among formulations. These differences cannot be fully characterized by a single modulus measurement at 28 days.

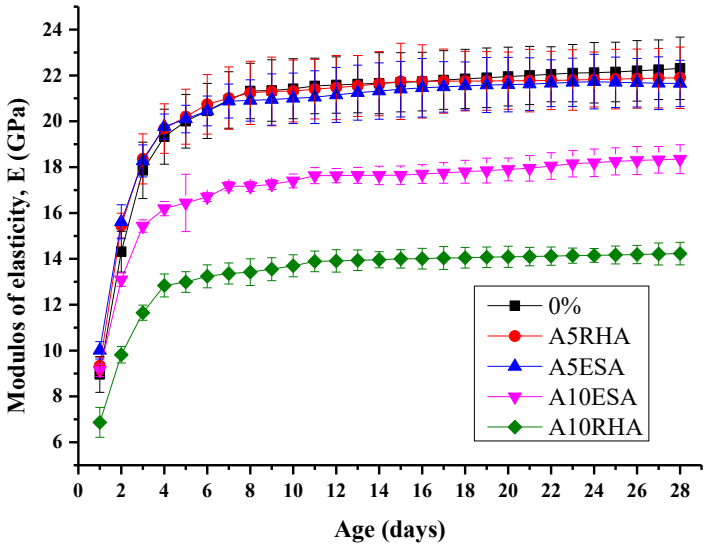


Figure 5. Dynamic elasticity modulus of mortar formulations over 28 days of curing (mean ± standard deviation; n = 5).

At 28 days, the reference mortar reached 22.31 ± 1.36 GPa, whereas A5%ESA and A5%RHA reached 21.65 ± 1.01 and 21.90 ± 1.34 GPa, corresponding to nominal reductions of approximately 3.0% and 1.8%, respectively. The values for A10%ESA and A10%RHA were 18.35 ± 0.63 and 14.23 ± 0.49 GPa, corresponding to reductions of approximately 17.8% and 36.2%.

Thus, the two 5% ash formulations retained final stiffness values close to the reference while exhibiting distinguishable temporal trajectories. Conversely, increasing the ash level to 10% was associated with lower final stiffness, most markedly for RHA.

Differences among formulations may reflect changes in particle packing, pore structure, and phase development associated with ash addition [13–20]. However, the present modulus data do not isolate these possible contributions, and no specific hydration mechanism is inferred.

The distinction between absolute modulus and the temporal trajectory motivates the normalized analysis in Section 3.4.

3.4. Normalized stiffness development and Avrami-type fitting

Figure 6 presents the normalized stiffness development index $\alpha_{E,28}$ and the corresponding Avrami-type fits. Normalization allows comparison of relative mechanical development independently of the absolute modulus attained by each formulation. The fitted adjusted R^2 values

ranged from 0.9875 to 0.9978, indicating satisfactory descriptive agreement within the experimental period. These values do not establish a unique physical hydration mechanism.

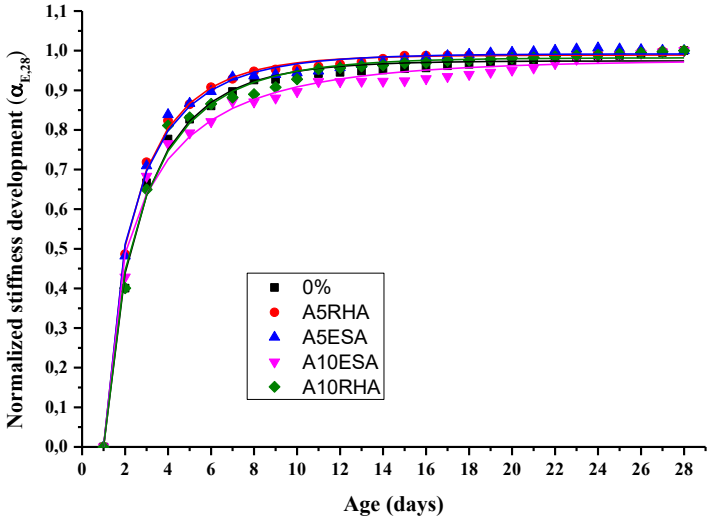


Figure 6. Normalized stiffness development index $\alpha_{E,28}$. Symbols: experimental mean values; lines: generalized Avrami-type fits.

Table 1 summarizes fitted parameters and characteristic times. The parameter uncertainties are standard errors from nonlinear fitting of mean trajectories, not standard deviations among specimens. The fitted asymptote A was not constrained to the normalized endpoint, so t_{50} and t_{90} represent fractions of A rather than fractions of the day-28 modulus.

Table 1. Generalized Avrami-type parameters fitted to mean normalized stiffness trajectories.

Formulation	*A*	*k* (day^{-1})	*n*	R^2adj	t_{50} (days)	t_{90} (days)
0%	0.9742 ± 0.0045	0.5340 ± 0.0180	0.8182 ± 0.0378	0.9938	2.20	6.19
A5%RHA	0.9889 ± 0.0026	0.6523 ± 0.0148	0.7722 ± 0.0232	0.9978	1.95	5.51
A5%ESA	0.9920 ± 0.0044	0.6471 ± 0.0246	0.7387 ± 0.0358	0.9942	1.94	5.78
A10%ESA	0.9765 ± 0.0101	0.5501 ± 0.0335	0.6128 ± 0.0447	0.9875	2.00	8.09
A10%RHA	0.9820 ± 0.0058	0.5259 ± 0.0220	0.7812 ± 0.0434	0.9911	2.19	6.53

Note: ± values for A, k, and n denote nonlinear-regression standard errors for fits to mean trajectories, not between-specimen standard deviations. Characteristic times refer to fractions of each fitted asymptote.

A5%RHA exhibited the highest apparent rate parameter, k = 0.6523 ± 0.0148 day^{-1}, followed by A5%ESA (0.6471 ± 0.0246 day^{-1}), compared with 0.5340 ± 0.0180 day^{-1} for the reference (0%). Characteristic times t_{90} were 5.51, 5.78, and 6.19 days, respectively. Thus, both 5% ash formulations

approached their own fitted stiffness-development asymptotes relatively faster than the reference, despite attaining similar absolute moduli at 28 days.

A10%ESA exhibited t_{50} = 2.00 days but the longest t_{90} (8.09 days), associated with n = 0.6128 and a more prolonged approach to its fitted asymptote. A10%RHA exhibited k = 0.5259 day^{-1} and t_{90} = 6.53 days, despite having the lowest final modulus. Accordingly, faster relative approach to a formulation-specific asymptote should not be interpreted as higher absolute stiffness or superior mechanical performance.

3.5. Apparent rate of stiffness development

Figure 7 presents the apparent rate calculated directly from finite differences between consecutive normalized experimental mean values and assigned to each interval midpoint. All formulations exhibited their largest rates during the first available interval, followed by a pronounced decrease. Initial rates for A5%RHA and A5%ESA were approximately 0.48 day^{-1}, compared with approximately 0.40 day^{-1} for the reference, consistent with their higher fitted k values and shorter characteristic times.

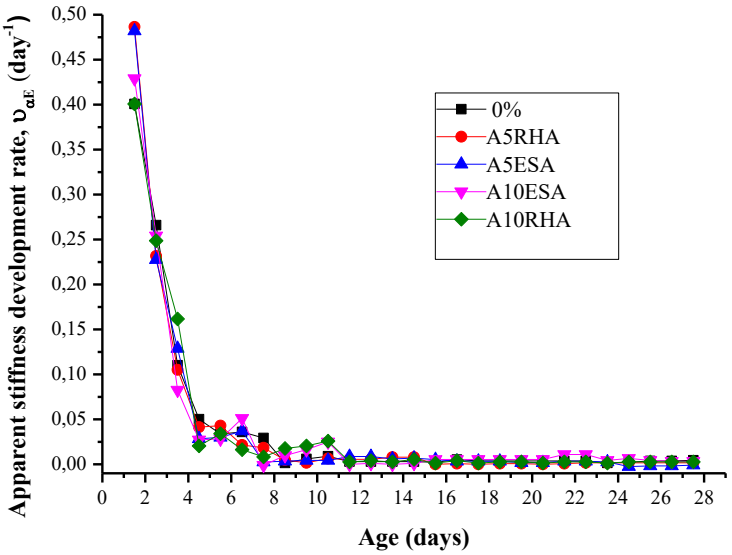


Figura 7. Apparent rate of normalized stiffness development, $\upsilon_{\alpha,E}$, calculated by finite differences and plotted at interval midpoints.

Small negative rates in some later intervals are consistent with experimental fluctuations when daily modulus changes become small; they must not be interpreted as a reversal of hydration. The calculated quantity is therefore described as an apparent stiffness-development rate rather than a

hydration rate. Figures 5–7 jointly demonstrate that ash addition modifies both the magnitude and relative temporal development of the mechanical response.

3.6. Physical and mechanical properties at 28 days

Table 2 summarizes apparent density, water absorption, apparent porosity, dynamic elastic modulus, modulus of rupture (MOR), and compressive strength at 28 days. The effects depended on ash type and addition level. Overall, 5% ash formulations exhibited properties closer to the reference, whereas 10% incorporation was associated with larger reductions in mechanical performance.

A5%ESA provided the most favorable overall balance. Compared with the reference, water absorption decreased from 16.26% to 13.92% (approximately 14.4%) and apparent porosity from 33.11% to 27.95% (approximately 15.6%), while apparent density changed from 2.02 to 2.00 g/cm³. Dynamic elastic modulus decreased nominally by approximately 3.0% and compressive strength by less than 0.3%, while MOR increased nominally by approximately 10.0%. In the absence of an inferential statistical comparison, these differences are reported as observed trends rather than statistically significant effects.

At 10% ESA incorporation, water absorption (14.94%) and apparent porosity (28.25%) remained below reference values, but apparent density fell to 1.89 g/cm³. Dynamic modulus, MOR, and compressive strength decreased by approximately 17.8%, 44.3%, and 29.8%, respectively. The fact that lower gravimetric apparent porosity was not accompanied by higher mechanical performance indicates that these physical indicators alone do not explain the load-bearing response.

Table 2. Apparent density, water absorption, apparent porosity, dynamic elastic modulus, flexural strength (MOR), and compressive strength at 28 days (mean ± standard deviation).

Formulation	Apparent density (g/cm³)	Water absorption (%)	Apparent porosity (%)	E (GPa)	MOR (MPa)	f_c (MPa)
0%	2.02 ± 0.02	16.26 ± 0.21	33.11 ± 0.41	22.31 ± 1.36	5.83 ± 0.33	23.76 ± 2.70
A5%ESA	2.00 ± 0.05	13.92 ± 0.36	27.95 ± 0.91	21.65 ± 1.01	6.41 ± 0.31	23.70 ± 1.80
A10%ESA	1.89 ± 0.08	14.94 ± 0.12	28.25 ± 0.99	18.35 ± 0.63	3.25 ± 0.31	16.67 ± 1.15
A5%RHA	1.97 ± 0.09	16.44 ± 0.99	33.51 ± 1.05	21.90 ± 1.34	5.44 ± 0.83	19.42 ± 1.97
A10%RHA	1.92 ± 0.15	17.94 ± 1.09	34.13 ± 1.28	14.23 ± 0.49	3.45 ± 0.40	17.59 ± 1.69

For A5%RHA, apparent density, absorption, and porosity remained close to reference values. Dynamic modulus decreased only 1.8% nominally, but MOR decreased by approximately 6.7% and compressive strength by 18.3%. Similar dynamic stiffness therefore did not imply equivalent flexural and compressive strengths.

A10%RHA exhibited water absorption of 17.94%, apparent porosity of 34.13%, and apparent density of 1.92 g/cm³. Compared with the reference, absorption increased approximately 10.3%, porosity 3.1%, and density decreased 5.0%. Dynamic modulus, MOR, and compressive strength decreased nominally by approximately 36.2%, 40.8%, and 26.0%, respectively.

The two ashes therefore influenced the measured properties differently. A5%RHA preserved stiffness close to the reference but showed lower compressive strength, whereas A5%ESA combined lower absorption and apparent porosity with stiffness and compressive strength near reference levels and a nominally higher MOR. Assessment of multiple properties is more informative than reliance on a single metric.

Considered alongside Sections 3.3–3.5, these results distinguish relative stiffness development from final mechanical performance. Both 5% ash formulations exhibited higher k and shorter t50/t90 than the reference, yet A5%RHA showed lower compressive strength. Likewise, the lower final modulus of the 10% formulations illustrates why characteristic times must be interpreted together with absolute stiffness.

The observed responses may involve particle packing, pore characteristics, or hydrated-phase development [13–20], but the present tests do not establish their individual contributions. Further work using pore-size and connectivity measurements, calorimetry, phase quantification, and microstructural analysis would be needed. Because ash was added without replacing cement while water-to-cement ratio remained constant, water-to-(cement + ash) ratio also varied across mixtures; the observed effects cannot be attributed exclusively to intrinsic ash reactivity.

From an applied perspective, these findings support careful consideration of both ash identity and dosage in waste-valorization strategies. The contribution of this study lies in linking physical and mechanical properties with experimentally monitored stiffness trajectories, while maintaining a distinction between phenomenological mechanical descriptors and direct measurements of hydration.

4. Conclusions

The additional incorporation of eggshell ash (ESA) and rice husk ash (RHA) modified the physical and mechanical properties and temporal stiffness development of cement mortars. The

effects depended on ash type and incorporation level. Under the investigated conditions, the 5% ash formulations generally provided a more favorable balance of properties than the 10% formulations.

A5%ESA exhibited the most favorable overall performance at 28 days. Compared with the reference, water absorption and apparent porosity decreased by approximately 14.4% and 15.6%, respectively. Dynamic elastic modulus was only 3.0% lower, compressive strength differed by less than 0.3%, and flexural strength showed a nominal increase of approximately 10.0%. These values describe experimental trends without implying statistical significance.

A5%RHA maintained a final dynamic elastic modulus close to the reference (nominally 1.8% lower), although compressive strength was approximately 18.3% lower. Increasing ash addition to 10% produced more pronounced reductions in mechanical performance; dynamic modulus decreased by approximately 17.8% for A10%ESA and 36.2% for A10%RHA relative to the reference.

Daily nondestructive monitoring showed the greatest stiffness increments at early ages, followed by progressively smaller increases. Normalization separated the relative temporal progression of stiffness from its absolute magnitude, complementing conventional testing at selected ages.

The generalized Avrami-type function described the mean normalized trajectories with adjusted R^2 between 0.9875 and 0.9978. A5%RHA and A5%ESA exhibited t90 values of 5.51 and 5.78 days, respectively, compared with 6.19 days for the reference. A10%ESA exhibited the longest t90 (8.09 days), indicating a more prolonged approach to its fitted asymptote.

Faster relative stiffness development did not necessarily correspond to higher final modulus or superior strength. Combining dynamic modulus monitoring, normalization, and phenomenological fitting provides complementary descriptors of temporal mechanical response. The Avrami-type parameters must not be interpreted as direct measurements of hydration degree or chemical reaction kinetics.

From an environmental perspective, the incorporation of relatively small amounts of agro-industrial ashes (5% relative to cement mass) represents a promising strategy for waste valorization in cementitious materials. Although the ashes were incorporated as additional constituents rather than as cement replacements, their inclusion increased the total solid mass and consequently reduced the relative cement fraction within the cement–ash system. At a 5% addition level, the cement fraction decreased from 100% to approximately 95.2% of the combined cement and ash mass, without reducing the absolute cement content. Particularly for ESA, this incorporation level also preserved mechanical performance close to that of the reference mortar while improving selected physical

properties. These findings highlight the potential of low-dosage ash incorporation to increase the use of secondary raw materials in cement mortars, although its net environmental benefits and potential to reduce cement consumption in practical applications require further assessment.

Overall, the results support the potential use of these ashes as additional constituents in cement mortars when ash type and dosage are carefully selected. Within the investigated conditions, 5% ESA provided the most favorable balance of physical properties, mechanical performance, and relative stiffness development. Direct hydration and microstructural studies would be required to establish the mechanisms responsible for the observed responses.

Acknowledgments

The authors gratefully acknowledge Prof. Dr. Elisângela de Jesus Cândido Moraes, graduate student Pedro Henrique Nunes, and technician Francisco Paiva for their valuable collaboration. The authors also acknowledge the financial support provided by the Brazilian National Council for Scientific and Technological Development (CNPq) through a Research Productivity Fellowship (Grant No. 313915/2021-0) and pre-undergraduate scientific research fellowships.

Data availability

The datasets generated and/or analysed during the current study are available from the corresponding author on reasonable request.

References

1. Lavagna, L. & Nisticò, R.. An insight into the chemistry of cement—a review. *Appl. Sci..* **13**, 203 (2023). https://doi.org/10.3390/app13010203

2. Nandhini, K. & Karthikeyan, J.. Sustainable and greener concrete production by utilizing waste eggshell powder as cementitious material—a review. *Constr. Build. Mater..* **335**, 127482 (2022). https://doi.org/10.1016/j.conbuildmat.2022.127482

3. Nandhini, K. & Karthikeyan, J.. Effective utilization of waste eggshell powder in cement mortar. *Mater. Today Proc..* **61**, 428–432 (2022). https://doi.org/10.1016/j.matpr.2021.11.328

4. Nehdi, M.L., Marani, A. & Zhang, L.. Is net-zero feasible: Systematic review of cement and concrete decarbonization technologies. *Renew. Sustain. Energy Rev..* **191**, 114169 (2024). https://doi.org/10.1016/j.rser.2023.114169

5. Hamada, H.M. & et al.. The present state of the use of eggshell powder in concrete: A review. *J. Build. Eng..* **32**, 101583 (2020). https://doi.org/10.1016/j.jobe.2020.101583

6. Kampragkou, P. & Stefanidou, M.. The role of different bio-additives in the properties of cement mortars. *Circ. Econ. Sustain.*. **5**, 7379–7387 (2025). https://doi.org/10.1007/s43615-025-00506-6

7. Zhao, X., Wang, H., Wang, X. & Zhao, X.. Sustainable application of waste eggshell as fillers in alkali-activated solid waste-based materials: Varying treated methods and particle sizes. *Constr. Build. Mater.*. **425**, 136040 (2024). https://doi.org/10.1016/j.conbuildmat.2024.136040

8. Nzereogu, P.U., Omah, A.D., Ezema, F.I., Iwuoha, E.I. & Nwanya, A.C.. Silica extraction from rice husk: Comprehensive review and applications. *Hybrid Adv.*. **4**, 100111 (2023). https://doi.org/10.1016/j.hybadv.2023.100111

9. Waheed, M. & et al.. Channelling eggshell waste to valuable and utilizable products: A comprehensive review. *Trends Food Sci. Technol.*. **106**, 78–90 (2020). https://doi.org/10.1016/j.tifs.2020.10.009

10. Ferraz, E., Gamelas, J.A.F., Coroado, J., Monteiro, C. & Rocha, F.. Eggshell waste to produce building lime: Calcium oxide reactivity, industrial, environmental and economic implications. *Mater. Struct.*. **51**, 115 (2018). https://doi.org/10.1617/s11527-018-1243-7

11. Consoli, N.C., Caicedo, A.M.L., Saldanha, R.B., Filho, H.C. Scheuermann & Acosta, C.J.M.. Eggshell produced limes: Innovative materials for soil stabilization. *J. Mater. Civ. Eng.*. **32**, 06020018 (2020). https://doi.org/10.1061/(ASCE)MT.1943-5533.0003418

12. (CONAB), Companhia Nacional de Abastecimento. Monitoring the Brazilian grain harvest: 2024/25 season [in Portuguese]. CONAB, Brasília, Brazil (2024).

13. He, Y., Che, D., Ouyang, X. & Niu, Y.. Surface properties of eggshell powder and its influence on cement hydration. *Materials.* **15**, 7633 (2022). https://doi.org/10.3390/ma15217633

14. Shiferaw, N., Habte, L., Thenepalli, T. & Ahn, J.W.. Effect of eggshell powder on the hydration of cement paste. *Materials.* **12**, 2483 (2019). https://doi.org/10.3390/ma12152483

15. Murthi, P., Lavanya, V. & Poongodi, K.. Effect of eggshell powder on structural and durability properties of high strength green concrete for sustainability: A critical review. *Mater. Today Proc.*. **68**, 1311–1318 (2022). https://doi.org/10.1016/j.matpr.2022.06.346

16. Tan, Y.Y., Doh, S.I. & Chin, S.C.. Eggshell as a partial cement replacement in concrete development. *Mag. Concr. Res.*. **70**, 662–670 (2018). https://doi.org/10.1680/jmacr.17.00003

17. Sathiparan, N.. Utilization prospects of eggshell powder in sustainable construction material—a review. *Constr. Build. Mater.*. **293**, 123465 (2021). https://doi.org/10.1016/j.conbuildmat.2021.123465

18. Ngayakamo, B. & Onwualu, A.P.. Recent advances in green processing technologies for valorisation of eggshell waste for sustainable construction materials. *Heliyon.* **8**, e09649 (2022). https://doi.org/10.1016/j.heliyon.2022.e09649

19. Tuan, N.V., Ye, G., Breugel, K. van, Fraaij, A.L.A. & Bui, D.D.. The study of using rice husk ash to produce ultra high performance concrete. *Constr. Build. Mater.*. **25**, 2030–2035 (2011). https://doi.org/10.1016/j.conbuildmat.2010.11.046

20. Madandoust, R. & Ghavidel, R.. Mechanical properties of concrete containing waste glass powder and rice husk ash. *Biosyst. Eng.*. **116**, 113–119 (2013). https://doi.org/10.1016/j.biosystemseng.2013.07.006

21. Zhao, H., Huang, D., Wang, X. & Chen, X.. Dynamic elastic modulus of cement paste at early age based on nondestructive test and multiscale prediction model. *J. Wuhan Univ. Technol.-Mater. Sci. Ed.*. **29**, 321–328 (2014). https://doi.org/10.1007/s11595-014-0915-6

22. Valentini, L. & et al.. Simulation of the hydration kinetics and elastic moduli of cement mortars by microstructural modelling. *Cem. Concr. Compos.*. **52**, 54–63 (2014). https://doi.org/10.1016/j.cemconcomp.2014.05.005

23. Bezjak, A.. Kinetic analysis of cement hydration including various mechanistic concepts. I. Theoretical development. *Cem. Concr. Res.*. **13**, 305–318 (1983). https://doi.org/10.1016/0008-8846(83)90029-7

24. Ma, B. & et al.. A simple cement hydration model considering the influences of water-to-cement ratio and mineral composition. *Comput. Model. Eng. Sci.*. **127**, 1059–1067 (2021). https://doi.org/10.32604/cmes.2021.015776

25. Thomas, J.J.. A new approach to modeling the nucleation and growth kinetics of tricalcium silicate hydration. *J. Am. Ceram. Soc.*. **90**, 3282–3288 (2007). https://doi.org/10.1111/j.1551-2916.2007.01858.x

26. Bishnoi, S. & Scrivener, K.L.. Studying nucleation and growth kinetics of alite hydration using μic. *Cem. Concr. Res.*. **39**, 849–860 (2009). https://doi.org/10.1016/j.cemconres.2009.07.004

27. ASTM International, ASTM C1198-91: Standard test method for dynamic modulus of elasticity, shear modulus, and Poisson's ratio for advanced ceramics by sonic resonance, ASTM International, West Conshohocken, PA (1991).

28. European Committee for Standardization (CEN), EN 1015-11:2019: Methods of test for mortar for masonry—Part 11: Determination of flexural and compressive strength of hardened mortar, CEN, Brussels (2019).

29. International Organization for Standardization (ISO), ISO 1920-4:2020: Testing of concrete—Part 4: Strength of hardened concrete, ISO, Geneva (2020).

30. ASTM International, ASTM C642-21: Standard test method for density, absorption, and voids in hardened concrete, ASTM International, West Conshohocken, PA (2021). https://doi.org/10.1520/C0642-21.